Quaternary Science Reviews 353 (2025) 109212

Contents lists available at ScienceDirect

Quaternary Science Reviews

journal homepage: www.elsevier.com/locate/quascirev

^{10}Be records of the Matuyama-Brunhes polarity reversal in the northeastern Chinese loess Plateau

Ling Tang [b], Weijian Zhou [a,c,d,*], Xisheng Wang [e], Feng Xian [a,c], Xianghui Kong [a,c], Yajuan Du [a,c], Jie Zhou [b], Guoqing Zhao [a,c], Yunchong Fu [a,c], Ning Chen [a,c]

[a] State Key Laboratory of Loess, Institute of Earth Environment, Chinese Academy of Sciences, Xi'an, 710061, China
[b] Xi'an Institute for Innovative Earth Environment Research, Xi'an, 710061, China
[c] Shaanxi Key Laboratory of AMS and Application, Xi'an AMS Center, Xi'an, 710061, China
[d] School of Human Settlements and Civil Engineering, Xi'an Jiaotong University, Xi'an, 710049, China
[e] Institute of Geomechanics, Chinese Academy of Geological Sciences, Beijing, 100081, China

A B S T R A C T

The precise stratigraphic position of the Matuyama-Brunhes (M-B) geomagnetic polarity reversal within Chinese loess sequences and its asynchrony with marine records have been long debated. This uncertainty limits our ability to establish a reliable geochronology for Chinese loess sequences and precise land-sea correlation of paleoclimate records. Here we present the high-resolution ^{10}Be results across the M-B boundary for the Fanshan loess profile in the northeastern Chinese Loess Plateau, for which previous high-stratigraphic-resolution paleomagnetic measurements failed to detect the exact position of the M-B boundary. A major enhancement of the ^{10}Be content (representing an increased atmospheric ^{10}Be production rate) in the upper part of paleosol S7 unambiguously represents the M-B boundary. The estimated age of 773 ± 3 ka for this boundary is consistent with ^{10}Be-inferred age of the M-B boundary in the EPICA Dome C ice core, marine sediment cores, and in the classic Luochuan loess sequence. These findings confirm the robustness of ^{10}Be in constraining geomagnetic reversals in Chinese loess sequences, after the effects of climate on ^{10}Be records have been successfully removed.

1. Introduction

Records of geomagnetic polarity reversals and excursions provide critical insights into the dynamic processes within the Earth's interior, and they are also key markers for global stratigraphic correlations. The Matuyama-Brunhes (M-B) geomagnetic polarity reversal at ~780 ka (Tauxe et al., 1996; Shackleton et al., 1990), is the key marker of the Lower/Middle Pleistocene boundary that facilitates correlations of sedimentary records worldwide (Heller and Evans, 1995; Zhou and Shackleton, 1999; Pan et al., 2001; Spassov et al., 2003; Zhu et al., 2006; Sun et al., 2013; Zhou et al., 2014). Chinese loess, together with ice cores and marine sediments, is regarded as one of the most important archives for documenting global climate change (Heller and Liu, 1982; Kukla and An, 1989; Zhang et al., 2022; Zhou et al., 2023b) and past geomagnetic field behavior (Pan et al., 2002; Liu et al., 2008; Yang et al., 2010; Zhou et al., 2014; Channell and Guyodo, 2004; Raisbeck et al., 2006; Valet et al., 2020). However, there is a long-standing debate on the fidelity of the paleomagnetic record of the M-B boundary in Chinese loess and marine sediments. This boundary is commonly encountered in glacial loess layer L8 in Chinese loess, corresponding to marine oxygen isotope stage (MIS) 20 (Liu et al., 1988; Rutter et al., 1991; Sun et al., 1998; Yang et al., 2004), but it is located in MIS 19 in marine sediments (Opdyke et al., 1966; Harrison, 1974; Zhou and Shackleton, 1999; Channell and Guyodo, 2004; Channell et al., 2010; Okada et al., 2017; Haneda et al., 2020). This apparent asynchrony hampers reliable land-ocean climatostratigraphic correlations. Although numerous studies have addressed the inconsistencies of the M-B boundary between Chinese loess and marine records (Liu et al., 2008; Jin and Liu, 2010), we still lack a clear understanding of the precise mechanism responsible for the spatiotemporal differences in the M-B boundary recorded by Chinese loess and marine sediments.

In addition to paleomagnetism, cosmogenic nuclides with suitable decay half-lives, like ^{10}Be, are a promising tool for documenting past variations in geomagnetic field intensity (Raisbeck et al., 2006; Valet

* Corresponding author. State Key Laboratory of Loess, Institute of Earth Environment, Chinese Academy of Sciences, Xi'an, 710061, China.
E-mail address: weijian@loess.llqg.ac.cn (W. Zhou).

https://doi.org/10.1016/j.quascirev.2025.109212
Received 27 August 2024; Received in revised form 6 January 2025; Accepted 20 January 2025
Available online 12 February 2025

et al., 2014; Simon et al., 2016). Due to the shielding effect of the geomagnetic field on cosmic ray penetration into the atmosphere, an inverse relationship between the production rate of cosmogenic ^{10}Be in the atmosphere and geomagnetic dipole strength has been quantitatively determined (Wagner et al., 2000; Muscheler et al., 2005; Masarik and Beer, 2009). The long radioactive decay half-life (Korschinek et al., 2010) and relatively short residence time of cosmogenic ^{10}Be in the atmosphere (~1–2 yr) (Ljung et al., 2007; Belmaker et al., 2008) make it possible to detect variations in geomagnetic field intensity, and therefore to detect geomagnetic reversals and excursions in ice cores (Wagner et al., 2000; Muscheler et al., 2005; Raisbeck et al., 2006; Berggren et al., 2009; Delaygue and Bard, 2011), marine sediments (Christl et al., 2003; Valet et al., 2014; Simon et al., 2016, 2018, 2020), loess deposits (Xian et al., 2008; Zhou et al., 2007, 2010, 2014), and lake sediments (Belmaker et al., 2008; Czymzik et al., 2015, 2016; Du et al., 2018; Tang et al., 2019). The advantage of the application of ^{10}Be to Chinese loess is that once deposited, ^{10}Be remains immobile within loess sections under natural conditions and is less affected by various post-depositional processes (Gu et al., 2000). Zhou et al. (2014) first used ^{10}Be to explore the stratigraphic position of the M-B boundary in Chinese loess and proposed that the M-B boundary was located within paleosol S7, corresponding to MIS 19, consistent with the position of the M-B boundary in marine sediments. A recent study by Zhou et al. (2023a), focusing on the Matuyama-Gauss boundary, further demonstrated the reliability of ^{10}Be for tracing geomagnetic reversals for Chinese Loess.

Pedogenic and climatic conditions vary spatially across the Chinese Loess Plateau (CLP), and thus it is essential to extend the application of ^{10}Be as a proxy of geomagnetic intensity variations in different areas on the CLP, and to evaluate its spatial and temporal variability and ability to reflect past geomagnetic field intensity. Previous investigations of the Fanshan loess section have revealed that loess-paleosol sequences are well-preserved in the northeastern CLP since ~1.2 Ma (Xiong et al., 2001). Unfortunately, a high-resolution paleomagnetic study revealed that the M-B boundary was not clearly recorded at Fanshan, either in L8 or S8. Instead, a clear normal-reverse polarity boundary was observed in the uppermost part of the upper loess layer (L9), indicating the significant downward displacement of the M-B boundary and extensive remagnetization (Wang et al., 2014). In the present study, we utilized parallel samples from a previous paleomagnetic study for cosmogenic ^{10}Be tracing, with the objective of detecting the M-B boundary. Our objectives were to accurately determine the stratigraphic position of the M-B boundary and then to evaluate possible factors contributing to any observed differences in the M-B boundary determined by ^{10}Be tracing and paleomagnetism. Our findings contribute to an improved understanding of the causes of the discrepancies in the stratigraphic position of the M-B boundary in various geological archives.

2. Site, methods, and ages

2.1. Site

The Fanshan loess section (40°11′40″N, 115°23′52″E) is located ~90 km northwest of Beijing (Fig. 1). Previous studies have shown that eolian deposits at Fanshan have continuously accumulated as early as 1.2 Ma (Xiong et al., 2001). The loess-paleosol sequences at this site have a homogenous texture and calcareous nodules occur sporadically throughout the profile, and they provide an opportunity to investigate the reliability of the paleomagnetic record of Chinese loess (Wang et al., 2014).

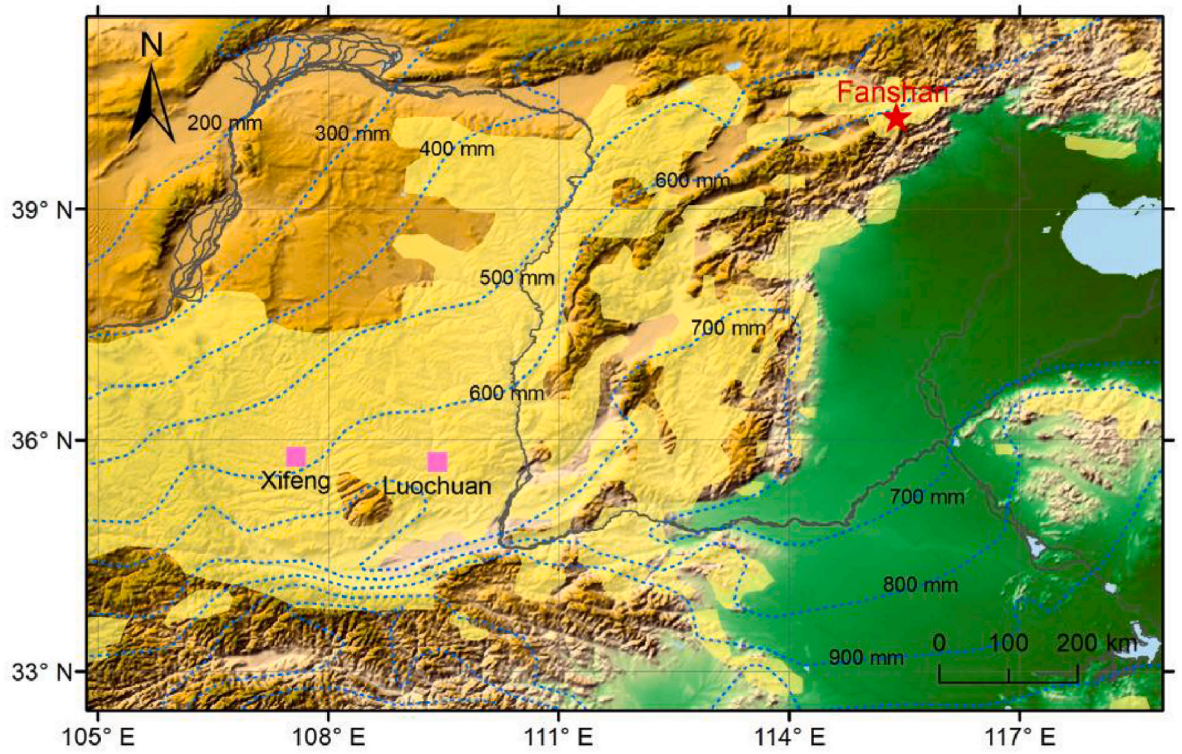

Fig. 1. Map showing the locations of the Fanshan, Xifeng, and Luochuan loess profiles. The mean annual precipitation isopleths are represented by dashed blue lines. The red star indicates the study site, and the pink squares indicate the Xifeng and Luochuan sites. (For interpretation of the references to colour in this figure legend, the reader is referred to the Web version of this article.)

2.2. Methods

We used previously collected loess subsamples spanning the interval from S6 to L9 for ^{10}Be measurements (Wang et al., 2014). A total of 150 samples were collected at an average spacing of 6 cm. The BeO samples were prepared at the Xi'an Accelerator Mass Spectrometry Center, where the ^{10}Be concentrations were measured (see Supplementary Information Chemical preparation). The background value for the ^{10}Be measurements was 3.65×10^{-15}, with a measurement error of ±3% (1σ) (Zhou et al., 2007).

2.3. Chronology

Loess-paleosol sequences provide a detailed record of climatic transitions between glacial and interglacial periods. Numerous studies have established the well-established correlation between the magnetic susceptibility stratigraphy of loess deposits and the marine oxygen isotope record (e.g., Heller and Liu, 1982; Heslop et al., 2000; Kukla and An, 1989; Sun et al., 2010). We utilized this correlation to develop a chronology for the Fanshan loess sequence. With reference to Heslop et al. (2000), we carefully correlated the Fanshan loess magnetic susceptibility profile with the stacked marine oxygen isotope record of Lisiecki and Raymo (2005), as illustrated in Supporting Information (SI) S1. The ages of the control points are given in Text S1 of SI. The ages between these control points were obtained by linear interpolation.

3. Results and discussion

3.1. Paleoclimatic influence on the ^{10}Be signal and extraction of ^{10}Be production rates

The ^{10}Be concentrations (^{10}Be$_{con}$) have the range of (128–541) × 10^6 atoms/g, and the peak values occur within S7 (Fig. 2a). The average value of 348 × 10^6 atoms/g across the interval of S6-L9 is higher than those at Xifeng (232 × 10^6 atoms/g) and Luochuan (285 × 10^6 atoms/g). ^{10}Be$_{con}$ covaries with the magnetic susceptibility (χ), the frequency-dependent susceptibility (χ$_{fd}$%), and the anhysteretic remanent magnetization (ARM), suggesting a strong climatic imprint on the ^{10}Be signal: high values occur in paleosols/weakly developed paleosols, and low values occur in loess layers (Fig. 2a–c). This observation is consistent with our understanding that the magnetic enhancement of Chinese loess is primarily due to the production of fine ferrimagnetic grains during pedogenesis (Zhou et al., 1990). Furthermore, it has been shown that the covariation of ^{10}Be$_{con}$ and χ is controlled mainly by variations in summer monsoon rainfall (Gu et al., 2000; Zhou et al., 2014). Previous studies show that the stratigraphic thickness between S6 and L9 at Fanshan is roughly equivalent to that of typical loess sections in the central Loess Plateau (Heller and Liu, 1982; Lu et al., 1999; Zhou et al., 2014). However, the peak χ values of the corresponding paleosols at Fanshan are lower than those in the classical loess-paleosol sequences at Xifeng and Luochuan (Fig. 2b, f, h). This indicates a weaker summer monsoon intensity in the northeastern CLP compared to the central CLP.

Generally, the ^{10}Be sequence in loess sections is an integrated signal of variations in climate and geomagnetic field intensity. Separating the climatically influenced component of ^{10}Be mainly depends on the selection of climate proxies. (Fig. 3a). Zhou et al. (2007) used a linear regression of ^{10}Be$_{con}$ *versus* χ to estimate the climatic component of ^{10}Be, based on the high correlation between χ and ^{10}Be$_{con}$ (Fig. 3b and c). To remove more effectively the climatic component of the ^{10}Be record, we conducted a correlation analysis between various magnetic parameters and ^{10}Be$_{con}$, aiming to extract reliable indicators that most closely represent the climate-related ^{10}Be component. The correlations between ARM, χ$_{fd}$%, and SIRM (saturation isothermal remanent magnetization) (which are roughly proportional to the concentration of magnetic minerals), and ARM/χ and ARM/SIRM (both of which are proxies of the ferrimagnetic grain size), and ^{10}Be$_{con}$. Among these parameters, ARM, ARM/SIRM, and χ$_{fd}$% have significant correlations with ^{10}Be$_{con}$ ($R > 0.6$), and χ$_{fd}$% and ARM/SIRM have even stronger correlations ($R > 0.7$) (Fig. 3d, f, h). The stronger correlations between these parameters and ^{10}Be$_{con}$ compared with that between χ and ^{10}Be$_{con}$ suggest that the fine ferrimagnetic minerals produced during pedogenesis are primarily influenced by the precipitation amount. We then extracted the common climatic signal from these parameters using principal component analysis (PCA). The first principal component (PC1) explained 96.7% of the variance, and it was selected as a climatic proxy to estimate the climatic component of ^{10}Be$_{con}$. The component of ^{10}Be$_{con}$ mainly modulated by the geomagnetic field intensity is represented by ^{10}Be-GM, with the calculation method detailed in Appendix S2.

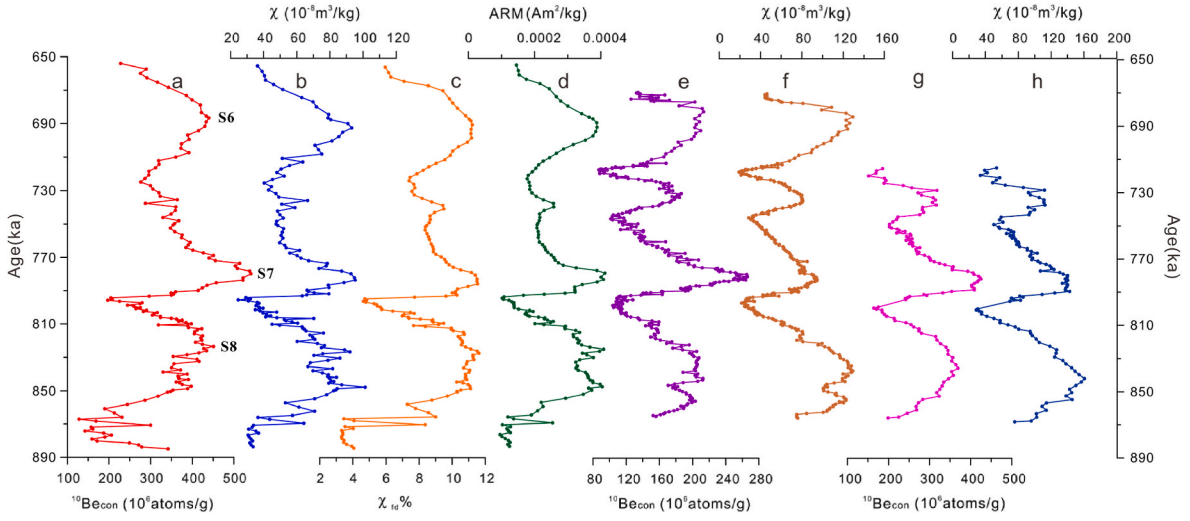

Fig. 2. Stratigraphic variations of ^{10}Be$_{con}$ and selected magnetic parameters. (a) ^{10}Be$_{con}$, (b) magnetic susceptibility (χ), (c) frequency-dependent magnetic susceptibility (χ$_{fd}$%), and (d) ARM of the Fanshan section (b–d) from Wang et al. (2014), (e–f) ^{10}Be$_{con}$ (purple curve) and χ (brown curve) from Xifeng, and ^{10}Be$_{con}$ (pink curve) and χ (blue curve) from Luochuan (g–h) over the interval of S6 to S9 (Zhou et al., 2014). (For interpretation of the references to colour in this figure legend, the reader is referred to the Web version of this article.)

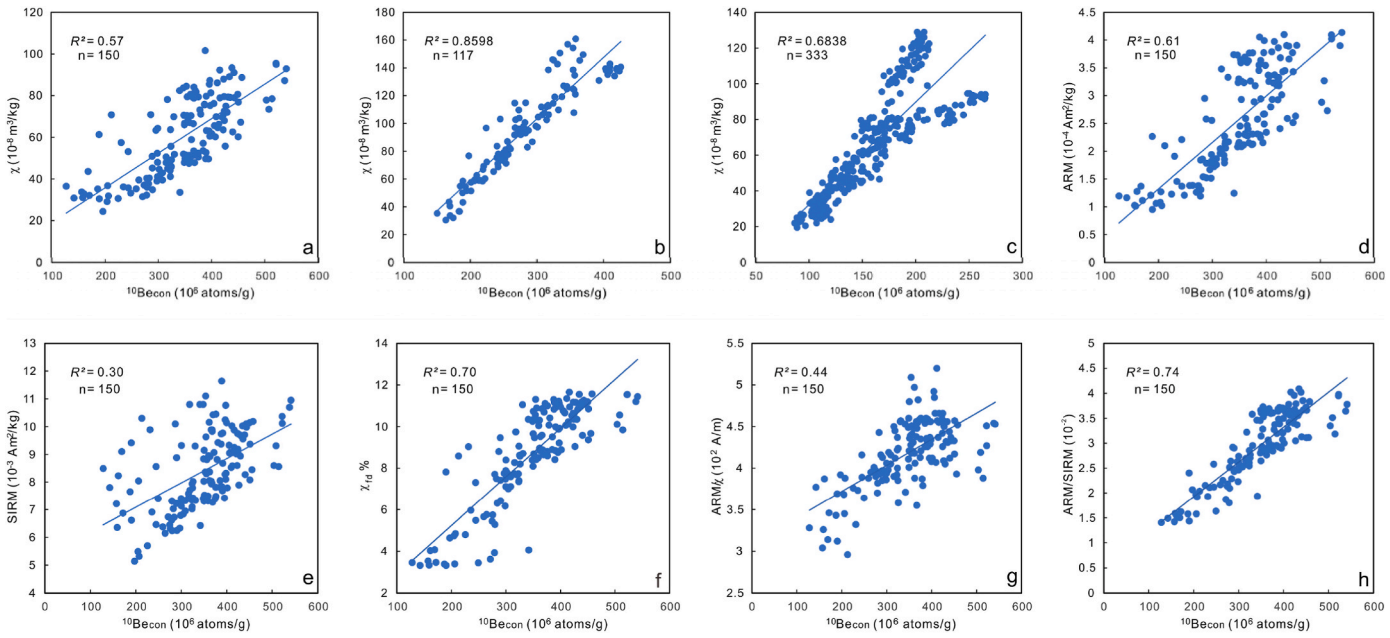

Fig. 3. Scatter plots of the relationship between magnetic susceptibility (χ) and $^{10}Be_{con}$ for (a) Fanshan, (b) Luochuan, and (c) Xifeng, and of the relationship between (d) ARM, (e) SIRM, (f) χ_{fd}%, (g) ARM/χ, and (h) ARM/SIRM and $^{10}Be_{con}$ for Fanshan. The correlations are significant at the 0.001 level.

3.2. Comparison of the M-B boundary in Chinese loess and other sedimentary archives

The rise in ^{10}Be-GM indicates a^{10}Be overproduction episode, with a prominent peak occurring in the upper part of S7 (Fig. 4a). Comparison of the timing of M-B reversal in other CLP sections and global geological records indicates that this ^{10}Be-GM peak represents the M-B boundary at Fanshan, which is centered at ~773 ± 3 ka, corresponding to MIS 19c. The relatively long duration of this ^{10}Be overproduction episode is also recorded in marine sedimentary records and the EPICA Dome C ice core, and it also corresponds to minimum virtual axial dipole moment (VADM) values in the SINT-2000 relative paleointensity stack. (Fig. 4a, d-h). Several paleomagnetic records show that the M-B boundary and its corresponding high-frequency polarity flips are widely recorded within L8-S8 on the CLP. Curiously, however, these features are not clearly documented across the M-B reversal in the Fanshan profile (Fig. 4c).

Although the ^{10}Be processing techniques, sampling intervals, and sedimentation rates for the three loess records are slightly different, the ^{10}Be-GM records show that the position of the M-B boundary traced by ^{10}Be is consistent in the three loess sections (Fig. 4a, j, l). However, outside the M-B boundary, there are slight differences in the variations of the ^{10}Be-GM curves among the three sections. Additionally, the position of the M-B boundary determined by ^{10}Be consistently falls within the upper part of S7, corresponding to the glacial inception of MIS 19c (Fig. 4i). While global geological records are generally chronologically aligned with the M-B boundary based on ^{10}Be data, discrepancies in its position and direction based on paleomagnetic techniques are largely due to differences in the recording quality of the primary remanent magnetization. The general consistency of the ^{10}Be-GM signal in the three loess profiles from different areas further confirms the validity of

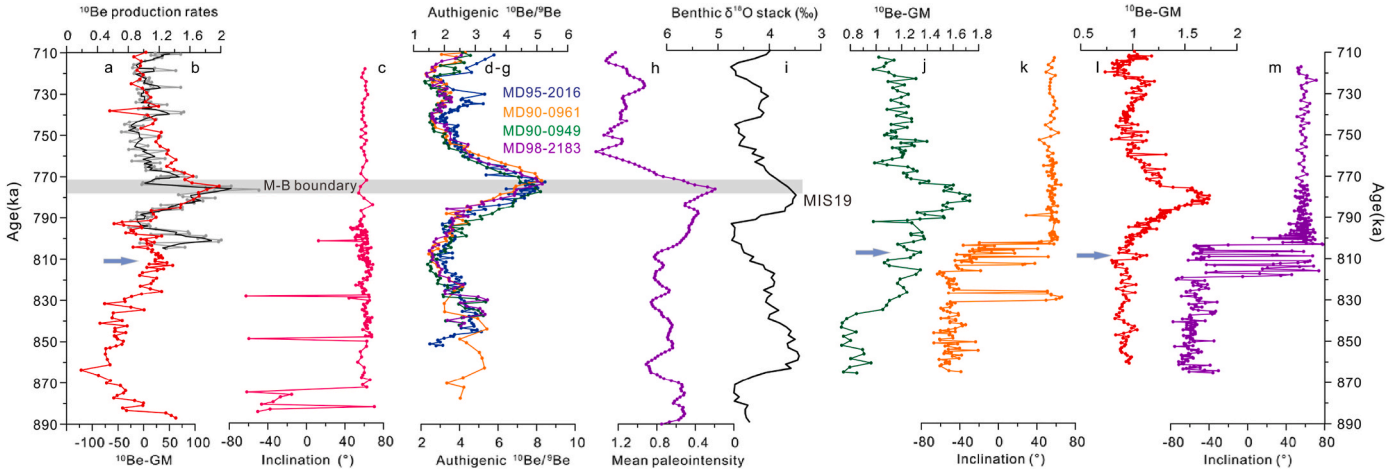

Fig. 4. Comparison of geomagnetic field records spanning 890–710 ka. (a) ^{10}Be-GM component recorded in the Fanshan loess section (red curve), (b) EPICA ice core ^{10}Be production signal (gray curve) and its three-point moving average (black curve) (Raisbeck et al., 2006), (c) Fanshan paleomagnetic inclination record (Wang et al., 2014), (d–g) Authigenic ^{10}Be/^{9}Be records in marine sediment cores MD95-2016 (blue curve), MD90-0961 (orange curve), MD90-0949 (green curve), and MD98-2183 (purple curve) (Simon et al., 2018), (h) SINT-2000 relative paleointensity stack (Valet et al., 2005), (i) benthic δ^{18}O stack (Lisiecki and Raymo, 2005), (j) Luochuan ^{10}Be-GM record, (k) Luochuan paleomagnetic inclination record, (l) Xifeng ^{10}Be-GM record, (m) Xifeng inclination record (Zhou et al., 2014). The blue arrow represents the 810 ka peak. (For interpretation of the references to colour in this figure legend, the reader is referred to the Web version of this article.)

cosmogenic nuclide techniques for tracing variations in geomagnetic field intensity.

Our new ^{10}Be-GM record resembles the SINT-2000 relative paleointensity stack (Fig. 4a, h), although there is a slight age offset between these two records, which could be caused either by uncertainties in the age models or by a possible post-depositional remanent magnetization (pDRM) lock-in effect of the relative paleointensity records. It is noteworthy that discrepancies persist between ^{10}Be records from Chinese loess and SINT-2000 based on multiple marine records, especially below the M-B boundary. It is also evident that the SINT-2000 record has lower geomagnetic field intensities prior to the B-M boundary compared to the subsequent time interval, while all these ^{10}Be records do not show this feature. The geomagnetic field intensity indicated by ^{10}Be data decays progressively from ~790 ka to B-M boundary, which is evident in both loess and marine records, whereas the SINT2000 relative paleointensity stack exhibits low-amplitude fluctuations (Fig. 4a, b, d-h). Furthermore, the SINT-2000 stack is derived from ten paleointensity records, each normalized by their respective mean values. Unlike relative magnetic paleointensity records that are likely overprinted by a secondary remanence, ^{10}Be sequences are typically less affected by various post-depositional processes in loess (Zhou and Shackleton, 1999). We therefore propose that ^{10}Be-derived paleointensity data can be incorporated into stacks of globally-distributed relative paleointensity records to accurately determine dipole field variations in future studies.

In addition to the M-B reversal, ^{10}Be records from various sedimentary records hint at a potential 'precursor event' ~18 kyr prior to the M-B transition (Singer et al., 2005; Channell et al., 2010). There is a conspicuous increase in the ^{10}Be concentration in the EDC ice core (Fig. 4b), representing the M-B precursor event marked by decreased relative paleointensity (Raisbeck et al., 2006; Simon et al., 2016). However, ^{10}Be records from Chinese loess do not show any significant increase during this time interval; instead, they all show a minor peak at ~810 ka (Fig. 4a, j, l). It is interesting that as Heqing Lake, a terrestrial sedimentary archive, there is a discernible, albeit slightly subdued, increase in ^{10}Be/^{9}Be ratios dating back to ~790–800 ka (Du et al., 2018). This enhancement in ^{10}Be/^{9}Be ratio notably precedes the M-B transition, suggesting its potential relevance for the chronology of the geomagnetic event. Certain ^{10}Be records from marine sediment cores also show a slight increase at around this time when the precursor event is thought to have occurred (Carcaillet et al., 2003; Suganuma et al., 2010). A notable decrease in paleomagnetic field intensity within the PISO-1500 dataset warrants further investigation, since the marine and loess ^{10}Be records do not corroborate an increase (Channell et al., 2009). However, the SINT-2000 relative paleointensity stack does not show a pronounced decrease in the geomagnetic dipole moment (GDM) in the corresponding region (Valet et al., 2005). The extent to which non-dipolar components amalgamated into collective records affect the overall pattern is unclear. Regardless of the possible complex transitional processes across the M-B, ^{10}Be data from three loess profiles on the CLP, together with those from marine sediments and EPICA ice core around the M-B boundary, highlight the ability of the ^{10}Be atmospheric production rate to accurately track variations in geomagnetic field intensity.

3.3. *Possible origin of the displacement of the M-B boundary in the Fanshan loess profile*

The acquisition and retention mechanisms of the primary remanence of Chinese loess in the margin of the CLP are complex (Wang et al., 2014). Previous high-resolution paleomagnetic studies at Fanshan showed that the M-B boundary was not clearly recorded between S7 and S8, while an abrupt reverse-to-normal polarity reversal is evident in the upper part of L9 (Fig. 4c; Wang et al., 2014). In contrast, as determined by thermal demagnetization, the M-B boundary is unambiguously confined to L8 at both Xifeng and Luochuan, although it occurs ~25 kyr earlier than their respective ^{10}Be-determined boundaries (Zhou et al., 2014). The systematically lower χ values at Fanshan indicate that the loess in the northeastern CLP has experienced weaker pedogenesis compared with Luochuan and Xifeng. The ternary diagram (Fig. S3) of Al_2O_3 - (CaO + Na_2O) - K_2O also reveals that the chemical index of alteration values of Fanshan are lower than those of Xifeng and Lingtai, suggesting that the Fanshan loess has undergone weaker chemical weathering compared to typical loess profiles in the central CLP. Previous studies of loess-paleosol sequences in the central and southern CLP showed that paleomagnetic signals across the M-B boundary are significantly influenced by pedogenesis, leading to a thinner L8 layer and an enhanced delayed lock-in effect (Liu et al., 2015). The M-B boundary can be readily identified in typical loess profiles such as Luochuan, Xifeng, Sanmenxia, and Lingtai (Heller and Liu, 1982; Wang et al., 2005, 2006, 2007; Liu et al., 2008), each of which experienced stronger pedogenesis compared to Fanshan. Therefore, we propose that a pedogenesis-related chemical remanent magnetization (CRM) and/or viscous remanent magnetization (VRM) may not be the primary mechanisms accounting for the significant downward displacement of the M-B boundary at Fanshan. For loess formed in a relatively humid environment, most magnetic particles become permanently locked-in after initial wetting. In the natural environment, repeated wetting caused by precipitation has the potential to generate a partial pDRM in loess deposits. This phenomenon can be further enhanced by physical disturbances such as bioturbation, collapse, and freeze-thaw processes (Løvlie and Putkonen, 1996). Considering that the Fanshan section is located at a higher latitude and has experienced greater temperature differences, of the order of 40 °C (Fig. S4), it is possible that the Fanshan loess may have undergone more intense freeze-thaw cycles compared to the other loess sections. During periods with geomagnetic reversals, a large decrease in the geomagnetic field intensity may also result in the decreased alignment efficiency of magnetic grains during the aforementioned processes. Along with the reduced stability of the geomagnetic field during a field reversal, the decreased alignment efficiency of the magnetic particles together with complex, localized remagnetization effects may lead to the absence and/or significant downward displacement of paleomagnetic polarity changes in the NE margin of the CLP (Løvlie et al., 2011; Wang et al., 2014).

4. Conclusions

Our high-resolution ^{10}Be analyses of the Fanshan loess profile in the NE CLP show that the stratigraphic position of the M-B polarity reversal should be located in paleosol S7, with the age of ~773 ± 3 ka (the MIS 19c interglacial), which is consistent with the ^{10}Be-derived age of the M-B boundary at the classical Luochuan and Xifeng loess records, marine sediments, and the EPICA Dome C ice core. Compared with the plethora of paleomagnetic results that show differences in the positions of geomagnetic reversals across the CLP, the ^{10}Be-derived geomagnetic field records appear to be minimally affected by post-depositional processes, and they are likely superior to paleomagnetism in determining the location of geomagnetic polarity boundaries in certain loess sequences. This result highlights the robustness of cosmogenic isotope records in tracing variations in geomagnetic field intensity and in constraining the stratigraphic position of geomagnetic reversals in loess sequences.

Author contribution

Ling Tang: Conceptualized the study, designed the ^{10}Be experiments, collected and analyzed the data, and wrote the manuscript, **Weijian Zhou**: Supervised the research, provided critical feedback, and contributed to the manuscript revision, **Xisheng Wang**: Provided samples and all environmental magnetic data, and contributed to the manuscript revision, **Jie Zhou, Guoqing Zhao**: Collected and analyzed the data, **Feng Xian, Xianghui Kong, Yajuan Du**: Contributed to the data interpretation and manuscript revision, **Yunchong Fu**: Data curation, **Ning Chen**: Provided critical feedback and helped shape the

research.

Declaration of competing interest

The authors declare that they have no known competing financial interests or personal relationships that could have appeared to influence the work reported in this paper.

Acknowledgements

This work was jointly supported by the National Natural Science Foundation of China (41930321), the National Natural Science Foundation of China (42102240), the Strategic Priority Research Program of the Chinese Academy of Sciences (XDB40010100), State Key Laboratory of Loess and Quaternary Geology, Institute of Earth Environment, CAS (SKLLQG 2023) and the National Natural Science Foundation of China (42103026).

Appendix A. Supplementary data

Supplementary data to this article can be found online at https://doi.org/10.1016/j.quascirev.2025.109212.

Data availability

All data and/or code is contained within the submission.

References

Belmaker, R., Lazar, B., Tepelyakov, N., Stein, M., Beer, J., 2008. ^{10}Be in Lake Lisan sediments -A proxy for production or climate? Earth Planet Sci. Lett. 269, 448–457.
Berggren, A.M., Beer, J., Possnert, G., Aldahan, A., Kubik, P., Christl, M., Johnsen, S.J., Abreu, J., Vinther, B.M., 2009. A 600-year annual ^{10}Be record from the NGRIP ice core, Greenland. Geophys. Res. Lett. 36, L11801.
Carcaillet, J.T., Thouveny, N., Bourlès, D.L., 2003. Geomagnetic moment instability between 0.6 and 1.3 Ma from cosmonuclide evidence. Geophys. Res. Lett. 30, 1792.
Channell, J.E.T., Guyodo, Y., 2004. The Matuyama chronozone at ODP site 982 (rockall bank): evidence for decimeter-scale magnetization lock-in depths. Timescales of The Paleomagnetic Field 205–219.
Channell, J.E.T., Hodell, D.A., Singer, B.S., Xuan, C., 2010. Reconciling astrochronological and ^{40}Ar/^{39}Ar ages for the Matuyama-Brunhes boundary and late Matuyama Chron. Geochem. Geophy. Geosy. 11, Q0AA12.
Channell, J.E.T., Xuan, C., Hodell, D.A., 2009. Stacking paleointensity and oxygen isotope data for the last 1.5 Myr (PISO-1500). Earth Planet Sci. Lett. 283, 14–23.
Christl, M., Strobl, C., Mangini, A., 2003. Beryllium-10 in deep-sea sediments: a tracer for the Earth's magnetic field intensity during the last 200,000 years. Quat. Sci. Rev. 22, 725–739.
Czymzik, M., Adolphi, F., Muscheler, R., Mekhaldi, F., Martin-Puertas, C., Aldahan, A., Possnert, G., Brauer, A., 2016. A varved lake sediment record of the ^{10}Be solar activity proxy for the Lateglacial-Holocene transition. Quat. Sci. Rev. 153, 31–39.
Czymzik, M., Muscheler, R., Brauer, A., Adolphi, F., Ott, F., Kienel, U., Dräger, N., Słowiński, M., Aldahan, A., Possnert, G., 2015. Solar cycles and depositional processes in annual ^{10}Be from two varved lake sediment records. Earth Planet Sci. Lett. 428, 44–51.
Delaygue, G., Bard, E., 2011. An Antarctic view of Beryllium-10 and solar activity for the past millennium. Clim. Dynam. 36, 2201–2218.
Du, Y.J., Zhou, W.J., Xian, F., Qiang, X.K., Kong, X.H., Zhao, G.Q., Xie, X.J., Fu, Y.C., 2018. ^{10}Be signature of the Matuyama-Brunhes transition from the Heqing paleolake basin. Quat. Sci. Rev. 199, 41–48.
Gu, Z.Y., Lal, D., Guo, Z.T., Liu, T., Southon, J., Caffee, M.W., 2000. Institute of Geology and geophysics. Geochemistry of cosmogenic ^{10}Be in loess-paleosol sequences and red clay in the Loess Plateau. Quat. Sci. 20, 409–422.
Haneda, Y., Okada, M., Suganuma, Y., Kitamura, T., 2020. A full sequence of the Matuyama–Brunhes geomagnetic reversal in the Chiba composite section, Central Japan. Prog. Earth Plant. Sci. 7, 44.
Harrison, C.G.A., 1974. The paleomagnetic record from deep-sea sediment cores. Earth Sci. Rev. 10, 1–36.
Heller, F., Evans, M.E., 1995. Loess magnetism. Rev. Geophys. 33, 211–240.
Heller, F., Liu, T., 1982. Magnetostratigraphical dating of loess deposits in China. Nature 300, 431–433.
Heslop, D., Langereis, C.G., Dekkers, M.J., 2000. A new astronomical timescale for the loess deposits of Northern China. Earth Planet Sci. Lett. 184, 125–139.
Jin, C.S., Liu, Q.S., 2010. Reliability of the natural remanent magnetization recorded in Chinese loess. J. Geophys. Res. Solid Earth 115, B04103.
Korschinek, G., Bergmaier, A., Faestermann, T., Gerstmann, U.C., Knie, K., Rugel, G., Wallner, A., Dillmann, I., Dollinger, G., Von Gostomski, C.L., Kossert, K., Maiti, M., Poutivtsev, M., Remmert, A., 2010. A new value for the half-life of ^{10}Be by Heavy-Ion Elastic Recoil Detection and liquid scintillation counting. Nucl. Instrum. Methods B 268, 187–191.
Kukla, G., An, Z.S., 1989. Loess stratigraphy in Central China. Palaeogeogr. Palaeocl. 72, 203–225.
Lisiecki, L.E., Raymo, M.E., 2005. Pliocene-Pleistocene stack of globally distributed benthic stable oxygen isotope records, Supplement to: Lisiecki, LE; Raymo, ME (2005): a Pliocene-Pleistocene stack of 57 globally distributed benthic δ^{18}O records. Paleoceanography 20, PA1003.
Liu, Q.S., Jin, C.S., Hu, P.X., Jiang, Z.X., Ge, K.P., Roberts, A.P., 2015. Magnetostratigraphy of Chinese loess–paleosol sequences. Earth Sci. Rev. 150, 139–167.
Liu, Q.S., Roberts, A.P., Rohling, E.J., Zhu, R.X., Sun, Y.B., 2008. Post-depositional remanent magnetization lock-in and the location of the Matuyama–Brunhes geomagnetic reversal boundary in marine and Chinese loess sequences. Earth Planet Sci. Lett. 275, 102–110.
Liu, X.M., Liu, T.S., Xu, T.C., Liu, C., Chen, M.Y., 1988. The Chinese loess in Xifeng, I. The primary study on magnetostratigraphy of a loess profile in Xifeng area, Gansu province. Geophys. J. Int. 92, 345–348.
Ljung, K., Björck, S., Muscheler, R., Beer, J., Kubik, P.W., 2007. Variable ^{10}Be fluxes in lacustrine sediments from Tristan da Cunha, South Atlantic: a solar record? Quat. Sci. Rev. 26, 829–835.
Løvlie, R., Putkonen, J., 1996. Dating of thaw depths in permafrost terrain by the palaeomagnetic method: experimental acquisition of a freezing remanent magnetization. Geophys. J. Int. 125, 850–856.
Løvlie, R., Wang, R., Wang, X., 2011. In situ remagnetization experiments of loess on the Chinese Loess Plateau: evidence for localized post-depositional remanent magnetization. Geochem. Geophy. Geosy. 12, 12.
Lu, H.Y., Liu, X.D., Zhang, F.Q., An, Z.S., Dodson, J., 1999. Astronomical calibration of loess–paleosol deposits at Luochuan, central Chinese Loess Plateau. Palaeogeogr. Palaeocl. 154, 237–246.
Masarik, J., Beer, J., 2009. An updated simulation of particle fluxes and cosmogenic nuclide production in the Earth's atmosphere. J. Geophys. Res. Atmos. 114, 1103.
Muscheler, R., Beer, J., Kubik, P.W., Synal, H.A., 2005. Geomagnetic field intensity during the last 60,000 years based on ^{10}Be and ^{36}Cl from the Summit ice cores and ^{14}C. Quat. Sci. Rev. 24, 1849–1860.
Okada, M., Suganuma, Y., Haneda, Y., Kazaoka, O., 2017. Paleomagnetic direction and paleointensity variations during the Matuyama–Brunhes polarity transition from a marine succession in the Chiba composite section of the Boso Peninsula, central Japan. Earth Planets Space 69, 45.
Opdyke, N., Glass, B., Hays, J., Foster, J., 1966. Paleomagnetic Study of Antarctic Deep-Sea Cores: paleomagnetic study of sediments in a revolutionary method of dating events in Earth's history. Science (New York, N.Y.) 154, 349–357.
Pan, Y.X., Zhu, R.X., Liu, Q.S., Yue, L.P., Wu, H.N., 2002. Geomagnetic episodes of the last 1.2 Myr recorded in Chinese loess. Geophys. Res. Lett. 29, 1282.
Pan, Y.X., Zhu, R.X., Shaw, J., Liu, Q.S., Guo, B., 2001. Can relative paleointensities be determined from the normalized magnetization of the wind-blown loess of China? J. Geophys. Res. Solid Earth 106, 19221–19232.
Raisbeck, G.M., Yiou, F., Cattani, O., Jouzel, J., 2006. ^{10}Be evidence for the Matuyama–Brunhes geomagnetic reversal in the EPICA Dome C ice core. Nature 444, 82–84.
Rutter, N., Ding, Z., Evans, M.E., Liu, T., 1991. Baoji-type pedostratigraphic section, Loess Plateau, north-central China. Quat. Sci. Rev. 10, 1–22.
Shackleton, N.J., Berger, A., Peltier, W.R., 1990. An alternative astronomical calibration of the lower Pleistocene timescale based on ODP Site 677. T. R. So. Edin. 81, 251–261.
Simon, Q., Thouveny, N., Bourlès, D.L., Bassinot, F., Savranskaia, T., Valet, J.P., 2018. Increased production of cosmogenic ^{10}Be recorded in oceanic sediment sequences: Information on the age, duration, and amplitude of the geomagnetic dipole moment minimum over the Matuyama–Brunhes transition. Earth Planet Sci. Lett. 489, 191–202.
Simon, Q., Thouveny, N., Bourlès, D.L., Valet, J.P., Bassinot, F., 2020. Cosmogenic ^{10}Be production records reveal dynamics of geomagnetic dipole moment (GDM) over the Laschamp excursion (20–60 ka). Earth Planet Sci. Lett. 550, 116547.
Simon, Q., Thouveny, N., Bourlès, D.L., Valet, J.P., Bassinot, F., Ménabréaz, L., Guillou, V., Choy, S., Beaufort, L., 2016. Authigenic ^{10}Be/^{9}Be ratio signatures of the cosmogenic nuclide production linked to geomagnetic dipole moment variation since the Brunhes/Matuyama boundary. J. Geophys. Res. Solid Earth 121, 7716–7741.
Singer, B.S., Hoffman, K.A., Coe, R.S., Brown, L.L., Jicha, B.R., Pringle, M.S., Chauvin, A., 2005. Structural and temporal requirements for geomagnetic field reversal deduced from lava flows. Nature 434, 633–636.
Spassov, S., Heller, F., Evans, M.E., Yue, L.P., Dobeneck, T.V., 2003. A lock-in model for the complex Matuyama-Brunhes boundary record of the loess/palaeosol sequence at Lingtai (Central Chinese Loess Plateau). Geophys. J. Int. 155, 350–366.
Suganuma, Y., Yokoyama, Y., Yamazaki, T., Kawamura, K., Horng, C.S., Matsuzaki, H., 2010. ^{10}Be evidence for delayed acquisition of remanent magnetization in marine sediments: implication for a new age for the Matuyama–Brunhes boundary. Earth Planet Sci. Lett. 296, 443–450.
Sun, D.H., Shaw, J., An, Z.S., Cheng, M.Y., Yue, L.P., 1998. Magnetostratigraphy and paleoclimatic interpretation of a continuous 7.2 Ma late cenozoic eolian sediments from the Chinese Loess Plateau. Geophys. Res. Lett. 25, 85–88.
Sun, Y.B., An, Z.S., Clemens, S.C., Bloemendal, J., Vandenberghe, J., 2010. Seven million years of wind and precipitation variability on the Chinese Loess Plateau. Earth Planet Sci. Lett. 297, 525–535.

Sun, Y.B., Qiang, X.K., Liu, Q.S., Bloemendal, J., Wang, X.L., 2013. Timing and lock-in effect of the Laschamp geomagnetic excursion in Chinese Loess. Geochem. Geophy. Geosy. 14, 4952–4961.

Tang, L., Zhou, W.J., Wang, X.S., Xian, F., Du, Y.J., Zhou, J., Chu, G.Q., Zhao, G.Q., Zhang, L., 2019. Multidecadal- to centennial-scale ^{10}Be variations in holocene sediments of huguangyan maar lake, south China. Geophys. Res. Lett. 46, 7634–7642.

Tauxe, L., Herbert, T., Shackleton, N.J., Kok, Y.S., 1996. Astronomical calibration of the Matuyama-Brunhes boundary: consequences for magnetic remanence acquisition in marine carbonates and the Asian loess sequences. Earth Planet Sci. Lett. 140, 133–146.

Valet, J.P., Bassinot, F., Bouilloux, A., Bourlès, D., Nomade, S., Guillou, V., Lopes, F., Thouveny, N., Dewilde, F., 2014. Geomagnetic, cosmogenic and climatic changes across the last geomagnetic reversal from Equatorial Indian Ocean sediments. Earth Planet Sci. Lett. 397, 67–79.

Valet, J.P., Meynadier, L., Guyodo, Y., 2005. Geomagnetic dipole strength and reversal rate over the past two million years. Nature 435, 802–805.

Valet, J.P., Thevarasan, A., Bassinot, F., Savranskaia, T., Haddam, N.A., 2020. Two records of relative paleointensity for the past 4 Myr. Front. Earth Sc-Switz 8, 148, 2020.

Wagner, G., Masarik, J., Beer, J., Baumgartner, S., Imboden, D., Kubik, P.W., Synal, H.A., Suter, M., 2000. Reconstruction of the geomagnetic field between 20 and 60 kyr BP from cosmogenic radionuclides in the GRIP ice core. Nucl. Instrum. Methods B 172, 597–604.

Wang, X.S., Løvlie, R., Chen, Y., Yang, Z.Y., Pei, J.L., Tang, L., 2014. The Matuyama–Brunhes polarity reversal in four Chinese loess records: high-fidelity recording of geomagnetic field behavior or a less than reliable chronostratigraphic marker? Quat. Sci. Rev. 101, 61–76.

Wang, X.S., Løvlie, R., Yang, Z.Y., Pei, J.L., Zhao, Z.Z., Sun, Z.M., 2005. Remagnetization of Quaternary eolian deposits: a case study from SE Chinese Loess Plateau. Geochem. Geophy. Geosy. 6, Q06H18.

Wang, X.S., Yang, Z.Y., Løvlie, R., Pei, J.L., Sun, Z.M., 2007. Discussion on the recording fidelity of the Matuyama/Brunhes boundary in the southeastern extremity of the Chinese loess plateau. Quat. Sci. 27, 963–971.

Wang, X.S., Yang, Z.Y., Løvlie, R., Sun, Z.M., Pei, J.L., 2006. A magnetostratigraphic reassessment of correlation between Chinese loess and marine oxygen isotope records over the last 1.1Ma. Phys. Earth Planet. In. 159, 109–117.

Xian, F., An, Z.S., Wu, Z.K., Beck, J.W., Yu, H.G., Kang, Z.H., Cheng, P., 2008. A simple model for reconstructing geomagnetic field intensity with ^{10}Be production rate and its application in Loess studies. Sci. China, Ser. A D 51, 855–861.

Xiong, S.F., Ding, Z.L., Liu, T., 2001. Climatic implications of loess deposits from the Beijing region. J. Quat. Sci. 16, 575–582.

Yang, T.S., Hyodo, M., Yang, Z.Y., Fu, J.L., 2004. Evidence for the kamikatsura and santa rosa excursions recorded in eolian deposits from the southern Chinese Loess Plateau. J. Geophys. Res. Solid Earth 109, B12105.

Yang, T.S., Hyodo, M., Yang, Z.Y., Li, H.D., Maeda, M., 2010. Multiple rapid polarity swings during the Matuyama-Brunhes transition from two high-resolution loess-paleosol records. J. Geophys. Res. Solid Earth 115, 101.

Zhang, J.J., Hao, Q.Z., Li, S.H., 2022. An absolutely dated record of climate change over the last three glacial–interglacial cycles from Chinese loess deposits. Geology 50, 1116–1120.

Zhou, L.P., Oldfield, F., Wintle, A.G., Robinson, S.G., Wang, J.T., 1990. Partly pedogenic origin of magnetic variations in Chinese loess. Nature 346, 737–739.

Zhou, L.P., Shackleton, N.J., 1999. Misleading positions of geomagnetic reversal boundaries in Eurasian loess and implications for correlation between continental and marine sedimentary sequences. Earth Planet Sci. Lett. 168, 117–130.

Zhou, W.J., Kong, X.H., Du, Y.J., Xie, X.J., Xian, F., Tang, L., Zhou, J., Zhao, G.Q., Fu, Y. C., Chen, N., 2023a. ^{10}Be indicator for the matuyama-gauss magnetic polarity reversal from Chinese loess. Geophys. Res. Lett. 50, e2022GL102486.

Zhou, W.J., Kong, X.H., Paterson, G.A., Sun, Y.B., Wu, Y.B., Ao, H., Xian, F., Du, Y.J., Tang, L., Zhou, J., Shi, Z.G., Jull, A.J.T., Zhao, G.Q., An, Z.S., 2023b. Eccentricity-paced geomagnetic field and monsoon rainfall variations over the last 870 kyr. P. Natl. A. Sci. 120, e2211495120.

Zhou, W.J., Priller, A., Beck, J.W., Wu, Z.K., Chen, M.B., An, Z.S., Kutschera, W., Xian, F., Yu, H.G., Liu, L., 2007. Disentangling geomagnetic and precipitation signals in an 80-kyr Chinese loess record of ^{10}Be. Radiocarbon 49, 137–158.

Zhou, W.J., Warren Beck, J., Kong, X.H., An, Z.S., Qiang, X.K., Wu, Z.K., Xian, F., Ao, H., 2014. Timing of the Brunhes-Matuyama magnetic polarity reversal in Chinese loess using ^{10}Be. Geology 42, 467–470.

Zhou, W.J., Xian, F., Beck, J.W., Jull, A.J.T., An, Z.S., Wu, Z.K., Liu, M., Chen, M.B., Priller, A., Kutschera, W., Burr, G.S., Yu, H.G., Song, S.H., Cheng, P., Kong, X.H., 2010. Reconstruction of 130-kyr relative geomagnetic intensities from ^{10}Be in two Chinese loess sections. Radiocarbon 52, 129–147.

Zhu, R.X., Liu, Q.S., Pan, Y.X., Deng, C.L., Zhang, R., Wang, X.F., 2006. No apparent lock-in depth of the Laschamp geomagnetic excursion: evidence from the Malan loess. Sci. China, Ser. A D 49, 960–967.